

Unveiling Non-Hermitian Spectral Topology in Hyperbolic Lattices with Non-Abelian Translation Symmetry

Mengying Hu*, Jing Lin, and Kun Ding†

Department of Physics, State Key Laboratory of Surface Physics, and Key Laboratory of Micro and Nano Photonic Structures (Ministry of Education), Fudan University, Shanghai 200438, China

*Email: myhu@fudan.edu.cn, †E-mail: kunding@fudan.edu.cn

Abstract

The hyperbolic lattice (HBL) has emerged as a compelling platform for exploring matter in non-Euclidean space. Among its notable features, the breakdown of the conventional Bloch theorem stands out, prompting a reexamination of band theory, with the determination of spectra for non-Hermitian systems being a prominent example. Here, we develop an approach to determining the spectra under open boundary conditions (OBCs), one of the foundations in non-Hermitian lattices, from the reciprocal space of HBLs. By introducing supercells to encompass states that are allowed by non-Abelian translational groups, we perform analytic continuation and base on the point gap topology to acquire uniform spectra, the universal OBC spectral range. Applying this method to a single-band nonreciprocal model and a reciprocal non-Abelian semimetal model, we reveal higher-dimensional skin effects and topological phase transitions, respectively, demonstrating the feasibility of our method in predicting spectral topology and investigating non-Hermitian physics in HBLs.

Introduction.—Recent years have witnessed a booming development of non-Hermitian physics[1-6], with myriad applications spanning classical waves[7-21], ultracold atoms[22-24], open quantum systems[25-27], and more[28,29]. The breakdown of Hermiticity introduces complex eigenenergies, resulting in spectral topology[5]. Unique to the non-Hermitian system, point gaps (PGs), characterized by eigenvalue winding numbers (EWNs), spontaneously emerge[2,30-35], while Hermitian systems only allow line gaps (LGs). Nontrivial PGs underpin the non-Hermitian skin effect (NHSE)[2,18,34-43], where bulk eigenstates localize at boundaries under open boundary conditions (OBCs) instead of extending as in Hermitian systems. Viewing NHSE from spectra indicates that the eigenenergies under periodic boundary conditions (PBCs) constitute PGs and vary remarkably under OBCs[34,35]. This discrepancy begs for the thermodynamic limit (TDL) OBC spectra calculation at the unit-cell level, breeding the celebrated non-Bloch band theory[2,44-47]. Although the spectral density of states (DOS) is sensitive to details, such as geometry and impurities[43,48-51], the universal OBC spectral range in arbitrary dimensions, denoted as σ_U , is crucial as it is rooted in the inherent PG topology [52,53]. Both the amoeba theory[52] and uniform spectra formulation[53] confirm σ_U , underscoring the central role of PGs and analytic continuation of Bloch wavenumbers in non-Hermitian physics.

However, the PG topology is fundamentally broader than that of Bloch wavenumbers, as PGs require only the existence of spectra, whereas Bloch wavenumbers rely on the translational group having one-dimensional (1D) irreducible representations (IRs)—a condition not always satisfied. Hyperbolic lattices (HBLs), constructed on a two-dimensional hyperbolic plane with constant negative curvature, exemplify such cases[54], differing from Euclidean lattices (ELs). Recent experimental achievements have positioned HBLs as a brilliant platform to investigate quantum matter in non-Euclidean geometries[55,56]. Hyperbolic counterparts of phenomena like topological insulators[57-63], Hofstadter states[57,64,65], flat bands[66-68], strong-correlated states[69,70], and Anderson localization[71,72] have been proposed, with some realized experimentally[58,60,61,63,70]. Exploring physics and phenomena unique to HBLs or lacking Euclidean analogs remains particularly compelling.

Unlike ELs, HBLs stand out due to negative curvature, and ensuingly, their translational groups, which are cornerstones in analyzing lattices, have been fundamentally altered[73]. Hyperbolic translation groups, known as Fuchsian groups, are non-Abelian and admit higher-dimensional IRs, necessitating a generalization of the Bloch theorem[74-76]. This demand makes

hyperbolic band theory (HBT) take shape, which incorporates Abelian [U(1)] and non-Abelian [U(d) for dimensions $d > 1$] components, corresponding to Abelian and non-Abelian Bloch states (NABSs)[74-80]. Determining the TDL spectra becomes first and foremost because the presence of NABSs invalidates standard EL approaches. Recently, several methods have been successfully established for forecasting Hermitian DOS under TDL, which reveals the criticality of NABSs [77,78]. While exceptional contours[81] and NHSEs[82-84] have been investigated in specific non-Hermitian HBLs, the general determination of uniform spectra σ_U with NABSs included remains an open and critical challenge.

To address this, we here formulate a systematic approach to determine σ_U for non-Hermitian HBLs. Our method utilizes incremental supercells to incorporate more NABSs and further employs analytic continuation to obtain σ_U . To illustrate, we first analyze a single-band model to contrast the PBC spectra and σ_U , thereby demonstrating the NHSE. We then delve into a celebrated non-Abelian semimetal model and reveal that NABSs exhibit distinct non-Hermitian phases compared with Abelian Bloch states (ABSs)[85].

Determination of uniform spectra.—To detail the conundrum of acquiring σ_U in HBLs, we commence from lattice tessellation to translation groups. Infinite lattices are typically tessellated into unit cells related by translational operations. Beyond using the smallest primitive cell, one can adopt specific groupings of $n (> 1)$ primitive cells, dubbed *n-supercell* ($n = 1$ being the primitive cell), to tile the lattice. Figures 1(a) and 1(b) depict the primitive cell, 2-supercell, and translational operators γ_i of a Euclidean {4,4} and hyperbolic {8,8} lattice (see details in Sec. I, Ref. [86]). PBCs compactify these cells into closed manifolds [bottom in Fig. 1(a,b)], referred to as PBC clusters. For an EL, any unit cell, regardless of n , is compactified to a torus [Fig. 1(a)]. However, for an HBL, the genus $g^{(n)} (= n(g^{(1)} - 1) + 1)$ of an n -supercell increases linearly with n , meaning different supercells are compactified onto manifolds with different genera[87,88]. For instance, the primitive cell and the 2-supercell in Fig. 1(b) are compactified onto surfaces with $g^{(1)} = 2$ and $g^{(2)} = 3$, respectively. This distinction reflects inherent differences in translation groups of HBLs and ELs[76].

Translational operations associated with primitive cells build the maximal translation group $\Gamma^{(1)} = \Gamma$, while those on n -supercells form subgroups $\Gamma^{(n)} \subset \Gamma^{(1)}$. The commutativity of $\gamma_i \in \Gamma^{(1)}$ in ELs ensures Abelian translation groups with only 1D IRs, forming the basis of the conventional Bloch theorem[89]. The n -supercells merely reduce the Brillouin zone size, resulting in band

folding without new physics, making primitive cell calculations sufficient in the TDL. In contrast, $\gamma_i \in \Gamma^{(1)}$ in HBLs generally do not commute, and translation groups allow higher-dimensional IRs[76]. These characterize states that cannot simply be modeled by a Bloch phase under translation, even with analytic continuations, thus defining NABSs[76]. Applying PBCs to the primitive cell only captures ABSs within the U(1)-HBT, which is insufficient for forecasting the TDL spectra. Employing n -supercells as PBC clusters enables the identification of NABSs because investigating $\Gamma^{(n)}$ can voluntarily invoke higher-dimensional IRs of Γ [78]. Hence, constructing a sequence of such PBC clusters to approach the TDL is then feasible and has shown a rapid convergence in the DOS for Hermitian systems as n increases, consistent with real-space calculations[77].

We now turn to the non-Hermitian scenario, where calculating σ_U is central. Since the essence of n -supercells lies in the necessity of examining $\Gamma^{(n)}$ as n increases, together with the fact that σ_U is based on the analytic continuation of Bloch wavenumbers into the complex plane, we next generalize the supercell method[78] to accommodate non-Hermitian HBLs. Wrapping the n -supercell into a PBC cluster requires implementing $d_{\{p,q\}}^{(n)}$ ($= 2g^{(n)}$) numbers of e^{ik_j} ($j = 1, \dots, d_{\{p,q\}}^{(n)}$) to specific pairs of boundaries (see details in Sec. I, Ref. [86]), and we perform $k_j \rightarrow k_j - i\mu_j$ for each k_j , leading to the n -supercell Hamiltonian $H^{(n)}(\beta_j = e^{ik_j + \mu_j})$. The EWNs are defined and now depend on n as follows[33-35]:

$$w_\alpha^{(n)}(E) = \int_0^{2\pi} \frac{dk_\alpha}{2\pi i} \partial_{k_\alpha} \ln f^{(n)}(E, \boldsymbol{\beta}^{(n)}), \quad (1)$$

where $E \in \mathbb{C}$ is the base energy, $\alpha = 1, \dots, d_{\{p,q\}}^{(n)}$, $f^{(n)}(E, \boldsymbol{\beta}^{(n)}) = \det[H^{(n)}(\boldsymbol{\beta}^{(n)}) - E]$ is the characteristic polynomial for the n -supercell, and $\boldsymbol{\beta}^{(n)} = \{\beta_j; j = 1, \dots, d_{\{p,q\}}^{(n)}\}$. The dependence of $w_\alpha^{(n)}(E)$ on k_α arises because winding numbers are defined over a parametric loop. Since nonzero EWNs forecast the occurrence of PGs, we introduce the rescaled spectrum of n -supercells as[35,53]:

$$\text{Sp}_\ell^{(n)}(|\beta_j|) = \{E; \sum_\alpha |w_\alpha^{(n)}(E)| \neq 0\}, \quad (2)$$

where each ℓ corresponds to a specific configuration of $|\beta_j|$ values. Physically, $\text{Sp}_\ell^{(n)}(|\beta_j|)$ identifies the spectral range with nonzero total EWNs for a given set of $|\beta_j|$ values[53]. The energy

residing in $\sigma_U^{(n)}$ requires that the total EWNs do not vanish for all $|\beta_j|$, or equivalently, PGs are nontrivially open [35]. Hence, $\sigma_U^{(n)}$ is obtained by taking the intersection of all $\text{Sp}_\ell^{(n)}(|\beta_j|)$ as

$$\sigma_U^{(n)} = \bigcap_{|\beta_j| \in (0, \infty), j} \text{Sp}_\ell^{(n)}(|\beta_j|). \quad (3)$$

Figure 1(c) sketches this intersection process, where three $\text{Sp}_\ell^{(n)}$ are shown as representatives of all $\text{Sp}_\ell^{(n)}$. The red hatched area, representing the intersection, corresponds to $\sigma_U^{(n)}$. Incrementing n then determine σ_U in non-Hermitian HBLs.

To demonstrate this approach, we first deploy the single-band models in the Euclidean {4,4} and hyperbolic {8,8} lattice. Figures 1(d) and 1(e,f) display the spectral ranges obtained from various n -supercells for the EL and HBL, respectively. The n -supercell PBC spectra $\sigma_P^{(n)}$ (grey areas) are calculated from the PBC cluster approach[78], while $\sigma_U^{(n)}$ (red areas) are obtained by our method. A common feature across Figs. 1(d-f) is $\sigma_U^{(n)} \subset \sigma_P^{(n)}$ for all n , a hallmark of NHSEs. As expected, the values of n do not alter $\sigma_P^{(n)}$ and $\sigma_U^{(n)}$ in the ELs [Fig. 1(d)], which aligns with the Abelian nature of $\Gamma^{(1)}$. Comparing Figs. 1(e) and 1(f) shows that $\sigma_P^{(n)}$ and $\sigma_U^{(n)}$ do not vary significantly with n , which is a consequence of the symmetry and nonreciprocity used in this concrete model (see details in Sec. II, Ref. [86]). We will later demonstrate the non-Abelian characteristic, where $\sigma_{P/U}^{(1)} \neq \sigma_{P/U}^{(n \neq 1)}$, highlighting the non-Abelian nature of $\Gamma^{(1)}$. Moreover, the observed differences between $\sigma_U^{(1)}$ and $\sigma_U^{(2)}$ illustrate the efficiency of our method (see details in Sec. II, Ref. [86]), further confirming the NHSE feature $\sigma_U^{(n)} \subset \sigma_P^{(n)}$. This result underscores that our method provides a systematic framework for investigating the spectral topology of HBLs, particularly the PG topology and phase transitions, which will be discussed next.

Higher-dimensional skin effects.—We first scrutinize the NHSE, a renowned manifestation of PG topology, to validate our recipe. Considering that higher-dimensional IRs possibly blur skin effects, we employ a particular kind of structure with meticulous boundary connections, which can be described using U(1)-HBT. As such, the primitive cell suffices to reflect the essential properties, and we name them as higher-dimensional Euclidean lattices (HDELs)[63]. To illustrate this, we deploy the nonreciprocal single-band model used in Fig. 1 on the HDEL and plot the spectra as blue circles in Fig. 2(a), which clearly reside within $\sigma_P^{(1)}$. By substituting quantized 4-dimensional momenta into $H^{(1)}(k_j)$, we compute the discretized PBC spectrum using U(1)-HBT, which aligns

perfectly with the blue circles in Fig. 2(a) (see details in Sec. II, Ref. [86]). This agreement confirms that $\sigma_p^{(1)}$ is sufficient for modeling HDELs, suggesting that the HDEL serves as an alternative platform for exploring non-Hermitian phenomena in high-dimensional Euclidean systems. The white and green lines in Fig. 2(a) represent the PBC spectra of the primitive cell by varying k_1 while fixing other k_j . Nontrivial PGs are clearly seen, and the occurrence of NHSE is forecasted.

By removing the PBC connections in the HDEL, we have the corresponding OBC structure, and the blue circles in Fig. 2(b) depict the calculated OBC spectra. For comparison, $\sigma_U^{(1)}$ from Fig. 1(e), which defines the spectral range where Abelian states can exist, is also shown. The OBC spectra lie within $\sigma_U^{(1)}$ and are noticeably distinct from the PBC spectra, suggesting NHSE. An exhibition of the nonreciprocal NHSE is the skewness of right and left eigenvectors[90,91]. We thus use the Kullback–Leibler (KL) divergence, a non-negative measure that quantifies the difference between two distributions, equaling 0 when they are identical and increasing with greater disparity[92]. The inset of Fig. 2(b) presents the percentage distribution of KL divergence between the right and left eigenvectors for states within the range highlighted by the white arrow, indicating the presence of NHSE.

Besides features in the eigenstates, NHSEs still highlight themselves as directional amplifications during transport[93-96]. Hence, for showcasing the NHSE, we choose to employ the Green’s function $G(E) = (E - H_{\text{OBC}})^{-1}$, where H_{OBC} is the OBC Hamiltonian, and E is an arbitrary energy. The upper panel of Fig. 2(c) illustrates the distribution of $|\langle p | G(E = 2.5) | s \rangle|$ as functions of s and p , wherein both are placed along the γ_1 direction, and the marker sizes are linearly proportional to their magnitudes. A clear tendency toward the negative γ_1 direction is seen, aligning with the spectral sum of eigenstates within the same range, as shown in the lower panel of Fig. 2(c). This tendency, together with the eigenstates, confirms the occurrence of NHSE, consistent with the nonreciprocal coupling direction. For comparison, Fig. 2(d) exhibits the distribution of $|\langle p | G(E = 2.5) | s \rangle|$ and the spectral sum of eigenstates along the γ_2 direction. No directional tendency is seen in the Green’s function, corroborating the absence of NHSE in the eigenstates. The contrast between the γ_1 and γ_2 directions attests to the NHSE and PG topology, verifying the implication of uniform spectra obtained by our method in HBLs.

Non-Abelian semimetals.—LGs, though also present in Hermitian systems, are as crucial as PGs for understanding eigenstate behaviors in non-Hermitian systems, as their spectral range closely relates to topological phase transitions in the eigenstates. Notably, it has been revealed in Hermitian HBLs that the emergence of NABSs can be even dominant over ABSs during such transitions[80]. To illustrate this, we employ the celebrated non-Abelian semimetal model on the $\{8,8\}$ lattice, defined as (see details in Sec. III, Ref. [86]):

$$H_{\text{OBC}} = \sum_{r,s} \left[\psi_r^\dagger \frac{\Gamma_5 - i\Gamma_s}{2} \psi_{r+s} + \text{h.c.} \right] + m \sum_r \psi_r^\dagger \Gamma_5 \psi_r, \quad (4)$$

where the spinor ψ_r has four components at each site $r \in \mathbb{Z}^4$, s ($= 1, \dots, 4$) corresponds to four translational directions, $\{\Gamma_v\}_{v=1}^5 = \{\sigma_1 \otimes \sigma_0, \sigma_2 \otimes \sigma_0, \sigma_3 \otimes \sigma_1, \sigma_3 \otimes \sigma_2, \sigma_3 \otimes \sigma_3\}$ with σ_v being the Pauli matrices, and $m \in \mathbb{C}$ ($= m_r + im_i$) denotes the onsite potential. When $m \in \mathbb{R}$, this model can be treated as the hyperbolic counterpart of the four-dimensional quantum Hall insulator in ELs, but the presence of NABSs spoils the LGs with nonzero second Chern numbers ($C_2 \neq 0$) from ABSs and makes it become semimetal. Concisely, at $m_r = 4$, the primitive cell (2-supercell) displays a topological phase transition from $C_2 \neq 0$ (semimetal) to a trivial insulator. Determining σ_U with NABSs included is now required to investigate how m_i alters the transitions, which are shown by the blue and red squares in Fig. 3(a). The left and right panels respectively depict results for the primitive cell and 2-supercell (see details in Sec. III, Ref. [86]). We can see that both transition points in m_r decrease when m_i climbs up, and thus, it can be expected that for a given m , $\sigma_U^{(2)}$ must show distinct behaviors compared with $\sigma_U^{(1)}$, a remarkable feature of NABSs.

We first choose $m = 3 + 0.3i$, which lies in the primitive cell gapped (2-supercell gapless) phase. The calculated $\sigma_U^{(1)}$ ($\sigma_U^{(2)}$) in Fig. 3(b) confirms that the LG is open (close) when non-Abelian states are absent (present). To further verify the origin of LG closing, we call U(2)-HBT[78,97] and show its spectra by grey dots in Fig. 3(b). Good agreement in the gap closing validates our method of σ_U and confirms that the spectral behaviors of non-Abelian states are from NABSs for reciprocal non-Hermitian systems (see Sec. III in Ref. [86]). We now turn to the trivial phase for both the primitive cell and the 2-supercell. Setting $m = 5 + 0.5i$, we clearly see a gap in $\sigma_U^{(1)}$ [Fig. 3(c)]. We also depict $\sigma_U^{(4)}$ in Fig. 3(c), which showcases that the LG remains intact in the TDL. However, the non-emptiness of $\sigma_U^{(4)} - \sigma_U^{(1)}$ hints at the appearance of non-Abelian states under OBCs. Thus, we compute the OBC spectra for two configurations, represented by the filled circles and stars in the inset of Fig. 3(c). Both OBC spectra lying in $\sigma_U^{(4)}$ validate our method of

acquiring σ_U , and degenerate states within $\sigma_U^{(4)} - \sigma_U^{(1)}$ affirm the existence of non-Abelian states. The distinction between the primitive cell and the n -supercell highlights the critical role of non-Abelian states in forming LGs and determining the OBC spectral range, further emphasizing the criticality of accurately calculating σ_U .

Discussions and conclusions.—In summary, we implement incremental supercells that can be wrapped into PBC clusters to encompass non-Abelian states and perform analytic continuation to determine uniform spectra in HBLs based on the connotation of PGs. By applying it to a single-band nonreciprocal model, we demonstrate higher-dimensional skin effects in an HDEL, showcasing the PG topology. Furthermore, through a non-Abelian semimetal model, our method successfully forecasts the topological phase transition points in both Abelian and non-Abelian states. Therefore, our approach offers a feasible way to investigate spectral topology and non-Hermitian phase transitions associated with gaps in HBLs. While our focus is on acquiring OBC spectra in the sense of TDL, the underlying principles of our method, which are based on subgroups and induced representations, can be generalized to other non-periodic lattices with well-defined generation groups, such as Cayley tree [98], Bethe lattice[99], and fractals[100]. Given recent advances in non-Hermitian topological invariants of higher-dimensional systems, regardless of whether non-Bloch [52] or real-space approaches[101,102] are employed, we believe our method is a valuable tool for investigating topological phase transitions and quantum phenomena in non-Hermitian HBLs.

Acknowledgment

We thank Prof. C. T. Chan and Mr. Nan Cheng for the helpful discussions. This work is supported by the National Key R&D Program of China (No. 2022YFA1404500, No. 2022YFA1404701), the National Natural Science Foundation of China (No. 12174072, No. 2021hwyq05), and the China Postdoctoral Science Foundation (No. 2023M730705).

References

- [1] R. El-Ganainy, K. G. Makris, M. Khajavikhan, Z. H. Musslimani, S. Rotter, and D. N. Christodoulides, *Non-Hermitian physics and PT symmetry*, Nat. Phys. **14**, 11 (2018).
- [2] S. Yao and Z. Wang, *Edge States and Topological Invariants of Non-Hermitian Systems*, Phys. Rev. Lett. **121**, 086803 (2018).
- [3] Y. Ashida, Z. Gong, and M. Ueda, *Non-Hermitian Physics*, Adv. Phys. **69**, 249 (2020).
- [4] E. J. Bergholtz, J. C. Budich, and F. K. Kunst, *Exceptional Topology of Non-Hermitian Systems*, Rev. Mod. Phys. **93**, 015005 (2021).
- [5] K. Ding, C. Fang, and G. Ma, *Non-Hermitian Topology and Exceptional-Point Geometries*, Nat. Rev. Phys. **4**, 745 (2022).
- [6] R. J. Lin, T. M. Y. Tai, L. H. Li, and C. H. Lee, *Topological non-Hermitian skin effect*, Frontier of Physics **18**, 53605 (2023).
- [7] A. Regensburger, C. Bersch, M. A. Miri, G. Onishchukov, D. N. Christodoulides, and U. Peschel, *Parity-time synthetic photonic lattices*, Nature **488**, 167 (2012).
- [8] L. Feng, Z. J. Wong, R. M. Ma, Y. Wang, and X. Zhang, *Single-mode laser by parity-time symmetry breaking*, Science **346**, 972 (2014).
- [9] B. Zhen, C. W. Hsu, Y. Igarashi, L. Lu, I. Kaminer, A. Pick, S.-L. Chua, J. D. Joannopoulos, and M. Soljačić, *Spawning Rings of Exceptional Points out of Dirac Cones*, Nature **525**, 354 (2015).
- [10] K. Ding, G. Ma, M. Xiao, Z. Q. Zhang, and C. T. Chan, *Emergence, Coalescence, and Topological Properties of Multiple Exceptional Points and Their Experimental Realization*, Phys. Rev. X **6**, 021007 (2016).
- [11] L. Feng, R. El-Ganainy, and L. Ge, *Non-Hermitian photonics based on parity-time symmetry*, Nat. Photonics **11**, 752 (2017).
- [12] H. Y. Zhou, C. Peng, Y. Yoon, C. W. Hsu, K. A. Nelson, L. Fu, J. D. Joannopoulos, M. Soljačić, and B. Zhen, *Observation of bulk Fermi arc and polarization half charge from paired exceptional points*, Science **359**, 1009 (2018).
- [13] M. A. Bandres, S. Wittek, G. Harari, M. Parto, J. H. Ren, M. Segev, D. N. Christodoulides, and M. Khajavikhan, *Topological insulator laser: Experiments*, Science **359**, eaar4005 (2018).
- [14] T. Ozawa *et al.*, *Topological photonics*, Rev. Mod. Phys. **91**, 015006 (2019).

- [15] W. Tang, X. Jiang, K. Ding, Y.-X. Xiao, Z.-Q. Zhang, C. T. Chan, and G. Ma, *Exceptional Nexus with a Hybrid Topological Invariant*, *Science* **370**, 1077 (2020).
- [16] H. R. Xue, Q. Wang, B. L. Zhang, and Y. D. Chong, *Non-Hermitian Dirac Cones*, *Phys. Rev. Lett.* **124**, 236403 (2020).
- [17] L. Zhang *et al.*, *Acoustic Non-Hermitian Skin Effect from Twisted Winding Topology*, *Nat. Commun.* **12**, 6297 (2021).
- [18] X. Zhang, T. Zhang, M.-H. Lu, and Y.-F. Chen, *A Review on Non-Hermitian Skin Effect*, *Adv. Phys. X* **7**, 2109431 (2022).
- [19] Q. C. Zhang, Y. T. Li, H. F. Sun, X. Liu, L. K. Zhao, X. L. Feng, X. Y. Fan, and C. Y. Qiu, *Observation of Acoustic Non-Hermitian Bloch Braids and Associated Topological Phase Transitions*, *Phys. Rev. Lett.* **130**, 017201 (2023).
- [20] Q. Y. Zhou, J. Wu, Z. H. Pu, J. Y. Lu, X. Q. Huang, W. Y. Deng, M. Z. Ke, and Z. Y. Liu, *Observation of geometry-dependent skin effect in non-Hermitian phononic crystals with exceptional points*, *Nat. Commun.* **14**, 4569 (2023).
- [21] J. Y. Lu, W. Y. Deng, X. Q. Huang, M. Z. Ke, and Z. Y. Liu, *Non-Hermitian Topological Phononic Metamaterials*, *Adv. Mater.* 2023, 2307998 (2023).
- [22] Q. Liang, D. Z. Xie, Z. L. Dong, H. W. Li, H. Li, B. Gadway, W. Yi, and B. Yan, *Dynamic Signatures of Non-Hermitian Skin Effect and Topology in Ultracold Atoms*, *Phys. Rev. Lett.* **129**, 070401 (2022).
- [23] Z. J. Ren, D. Liu, E. T. Zhao, C. D. He, K. K. Pak, E. S. Li, and G. B. Jo, *Chiral control of quantum states in non-Hermitian spin-orbit-coupled fermions*, *Nat. Phys.* **18**, 385 (2022).
- [24] R. Rosa-Medina, F. Ferri, F. Finger, N. Dogra, K. Kroeger, R. Lin, R. Chitra, T. Donner, and T. Esslinger, *Observing Dynamical Currents in a Non-Hermitian Momentum Lattice*, *Phys. Rev. Lett.* **128**, 143602 (2022).
- [25] L. Pan, X. Chen, Y. Chen, and H. Zhai, *Non-Hermitian linear response theory*, *Nat. Phys.* **16**, 767 (2020).
- [26] T. Haga, M. Nakagawa, R. Hamazaki, and M. Ueda, *Slowing Down of Relaxation Processes without Gap Closing*, *Phys. Rev. Lett.* **127**, 070402 (2022).
- [27] J. T. Bu *et al.*, *Enhancement of Quantum Heat Engine by Encircling a Liouvillian Exceptional Point*, *Phys. Rev. Lett.* **130**, 110402 (2023).

- [28] H. T. Shen and L. Fu, *Quantum Oscillation from In-Gap States and a Non-Hermitian Landau Level Problem*, Phys. Rev. Lett. **121**, 026403 (2018).
- [29] T. Yoshida, R. Peters, and N. Kawakami, *Non-Hermitian perspective of the band structure in heavy-fermion systems*, Phys. Rev. B **98**, 035141 (2018).
- [30] Z. Gong, Y. Ashida, K. Kawabata, K. Takasan, S. Higashikawa, and M. Ueda, *Topological Phases of Non-Hermitian Systems*, Phys. Rev. X **8**, 031079 (2018).
- [31] H. Shen, B. Zhen, and L. Fu, *Topological Band Theory for Non-Hermitian Hamiltonians*, Phys. Rev. Lett. **120**, 146402 (2018).
- [32] K. Kawabata, T. Bessho, and M. Sato, *Classification of Exceptional Points and Non-Hermitian Topological Semimetals*, Phys. Rev. Lett. **123**, 066405 (2019).
- [33] K. Kawabata, K. Shiozaki, M. Ueda, and M. Sato, *Symmetry and Topology in Non-Hermitian Physics*, Phys. Rev. X **9**, 041015 (2019).
- [34] K. Zhang, Z. Yang, and C. Fang, *Correspondence between Winding Numbers and Skin Modes in Non-Hermitian Systems*, Phys. Rev. Lett. **125**, 126402 (2020).
- [35] N. Okuma, K. Kawabata, K. Shiozaki, and M. Sato, *Topological Origin of Non-Hermitian Skin Effects*, Phys. Rev. Lett. **124**, 086801 (2020).
- [36] F. K. Kunst, E. Edvardsson, J. C. Budich, and E. J. Bergholtz, *Biorthogonal Bulk-Boundary Correspondence in Non-Hermitian Systems*, Phys. Rev. Lett. **121**, 026808 (2018).
- [37] C. H. Lee and R. Thomale, *Anatomy of skin modes and topology in non-Hermitian systems*, Phys. Rev. B **99**, 201103 (2019).
- [38] D. S. Borgnia, A. J. Kruchkov, and R.-J. Slager, *Non-Hermitian Boundary Modes and Topology*, Phys. Rev. Lett. **124**, 056802 (2020).
- [39] A. Ghatak, M. Brandenbourger, J. van Wezel, and C. Coulais, *Observation of non-Hermitian topology and its bulk-edge correspondence in an active mechanical metamaterial*, Proc. Natl. Acad. Sci. U.S.A. **117**, 29561 (2020).
- [40] T. Helbig *et al.*, *Generalized bulk-boundary correspondence in non-Hermitian topoelectrical circuits*, Nat. Phys. **16**, 747 (2020).
- [41] L. Xiao, T. S. Deng, K. K. Wang, G. Y. Zhu, Z. Wang, W. Yi, and P. Xue, *Non-Hermitian bulk-boundary correspondence in quantum dynamics*, Nat. Phys. **16**, 761 (2020).
- [42] W. Wang, X. Wang, and G. Ma, *Non-Hermitian Morphing of Topological Modes*, Nature **608**, 50 (2022).

- [43] K. Zhang, Z. Yang, and C. Fang, *Universal Non-Hermitian Skin Effect in Two and Higher Dimensions*, Nat. Commun. **13**, 2496 (2022).
- [44] F. Song, S. Yao, and Z. Wang, *Non-Hermitian Topological Invariants in Real Space*, Phys. Rev. Lett. **123**, 246801 (2019).
- [45] K. Yokomizo and S. Murakami, *Non-Bloch Band Theory of Non-Hermitian Systems*, Phys. Rev. Lett. **123**, 066404 (2019).
- [46] K. Kawabata, N. Okuma, and M. Sato, *Non-Bloch band theory of non-Hermitian Hamiltonians in the symplectic class*, Phys. Rev. B **101**, 195147 (2020).
- [47] Z. S. Yang, K. Zhang, C. Fang, and J. P. Hu, *Non-Hermitian Bulk-Boundary Correspondence and Auxiliary Generalized Brillouin Zone Theory*, Phys. Rev. Lett. **125**, 226402 (2020).
- [48] W. Wang, M. Y. Hu, X. L. Wang, G. C. Ma, and K. Ding, *Experimental Realization of Geometry-Dependent Skin Effect in a Reciprocal Two-Dimensional Lattice*, Phys. Rev. Lett. **131**, 207201 (2023).
- [49] C. Shu, K. Zhang, and K. Sun, *Ultra spectral sensitivity and non-local bi-impurity bound states from quasi-long-range non-hermitian skin modes*, arXiv: 2409.13623.
- [50] K. Zhang, C. Shu, and K. Sun, *Algebraic non-Hermitian skin effect and unified non-Bloch band theory in arbitrary dimensions*, arXiv:2406.06682.
- [51] F. Song, H.-Y. Wang and Z. Wang, *Fragile non-Bloch spectrum and unconventional Green's function*, arXiv:2410.23175.
- [52] H.-Y. Wang, F. Song, and Z. Wang, *Amoeba Formulation of Non-Bloch Band Theory in Arbitrary Dimensions*, Phys. Rev. X **14**, 021011 (2024).
- [53] H. Hu, *Topological origin of non-Hermitian skin effect in higher dimensions and uniform spectra*, Sci. Bull. (Beijing) **24**, 00502-4(2024)
- [54] Coxeter, H. S. M., *Crystal symmetry and its generalizations*, Proc. Trans. R. Soc. Can. **51**, 1 (1957).
- [55] A. J. Kollár, M. Fitzpatrick, and A. A. Houck, *Hyperbolic lattices in circuit quantum electrodynamics*, Nature **571**, 45 (2019).
- [56] P. M. Lenggenhager *et al.*, *Simulating hyperbolic space on a circuit board*, Nat. Commun. **13**, 4373 (2022).

- [57] S. Yu, X. Piao, and N. Park, *Topological Hyperbolic Lattices*, Phys. Rev. Lett. **125**, 053901 (2020).
- [58] W. Zhang, H. Yuan, N. Sun, H. Sun, and X. Zhang, *Observation of novel topological states in hyperbolic lattices*, Nat. Commun. **13**, 2937 (2022).
- [59] Z.-R. Liu, C.-B. Hua, T. Peng, and B. Zhou, *Chern insulator in a hyperbolic lattice*, Phys. Rev. B **105**, 245301 (2022).
- [60] W. Zhang, F. Di, X. Zheng, H. Sun, and X. Zhang, *Hyperbolic band topology with non-trivial second Chern numbers*, Nat. Commun. **14**, 1083 (2023).
- [61] Q. Pei, H. Yuan, W. Zhang, and X. Zhang, *Engineering boundary dominated topological states in defective hyperbolic lattices*, Phys. Rev. B **107**, 165145 (2023).
- [62] A. F. Y. Chen, Y. F. Guan, P. M. Lenggenger, J. Maciejko, I. Boettcher, and T. Bzdusek, *Symmetry and topology of hyperbolic Haldane models*, Phys. Rev. B **108**, 085114 (2023).
- [63] A. Chen *et al.*, *Hyperbolic matter in electrical circuits with tunable complex phases*, Nat. Commun. **14**, 622 (2023).
- [64] K. Ikeda, S. Aoki, and Y. Matsuki, *Hyperbolic band theory under magnetic field and Dirac cones on a higher genus surface*, J. Phys.: Condens. Matter **33**, 485602 (2021).
- [65] A. Stegmaier, L. K. Upreti, R. Thomale, and I. Boettcher, *Universality of Hofstadter Butterflies on Hyperbolic Lattices*, Phys. Rev. Lett. **128**, 166402 (2022).
- [66] A. J. Kollár, M. Fitzpatrick, P. Sarnak, and A. A. Houck, *Line- Graph Lattices: Euclidean and Non-Euclidean Flat Bands, and Implementations in Circuit Quantum Electrodynamics*, Commun. Math. Phys. **376**, 1909 (2020).
- [67] T. Bzdusek and J. Maciejko, *Flat bands and band-touching from real-space topology in hyperbolic lattices*, Phys. Rev. B **106**, 155146 (2022).
- [68] R. Mosseri, R. Vogeler, and J. Vidal, *Aharonov-Bohm cages, flat bands, and gap labeling in hyperbolic tilings*, Phys. Rev. B **106**, 155120 (2022).
- [69] X. Zhu, J. Guo, N. P. Breuckmann, H. Guo, and S. Feng, *Quantum phase transitions of interacting bosons on hyperbolic lattices*, J. Phys.: Condens. Matter **33**, 335602 (2021).
- [70] P. Bienias, I. Boettcher, R. Belyansky, A. J. Kollár, and A. V. Gorshkov, *Circuit Quantum Electrodynamics in Hyperbolic Space: From Photon Bound States to Frustrated Spin Models*, Phys. Rev. Lett. **128**, 013601 (2022).

- [71] A. Chen, J. Maciejko, and I. Boettcher, *Anderson Localization Transition in Disordered Hyperbolic Lattices*, Phys. Rev. Lett. **133**, 066101 (2024).
- [72] T. Y. Li, Y. Peng, Y. C. Wang, and H. P. Hu, *Anderson transition and mobility edges on hyperbolic lattices with randomly connected boundaries*, Commun. Phys. **7**, 371(2024).
- [73] I. Boettcher, A. V. Gorshkov, A. J. Kollar, J. Maciejko, S. Rayan, and R. Thomale, *Crystallography of hyperbolic lattices*, Phys. Rev. B **105**, 125118 (2022).
- [74] J. Maciejko and S. Rayan, *Hyperbolic band theory*, Sci. Adv. **7**, abe9170 (2021).
- [75] N. Cheng, F. Serafin, J. McInerney, Z. Rocklin, K. Sun, and X. Mao, *Band Theory and Boundary Modes of High-Dimensional Representations of Infinite Hyperbolic Lattices*, Phys. Rev. Lett. **129**, 088002 (2022).
- [76] J. Maciejko and S. Rayan, *Automorphic Bloch theorems for hyperbolic lattices*, Proc. Natl. Acad. Sci. U.S.A. **119** (2022).
- [77] R. Mosseri and J. Vidal, *Density of states of tight-binding models in the hyperbolic plane*, Phys. Rev. B **108**, 035154 (2023).
- [78] P. M. Lenggenhager, J. Maciejko, and T. Bzdusek, *Non-Abelian hyperbolic band theory from supercells*, Phys. Rev. Lett. **131**, 226401 (2023).
- [79] F. R. Lux and E. Prodan, *Spectral and Combinatorial Aspects of Cayley-Crystals*, Ann. Henri. Poincare **25**, 3563 (2024).
- [80] T. Tummuru, A. Chen, P. M. Lenggenhager, T. Neupert, J. Maciejko, and T. Bzduek, *Hyperbolic Non-Abelian Semimetal*, Phys. Rev. Lett. **132**, 206601 (2024).
- [81] N. Chadha and A. Narayan, *Uncovering exceptional contours in non-Hermitian hyperbolic lattices*, J. Phys. A-Math. Theor. **57**, 115203 (2024).
- [82] C. W. Lv, R. Zhang, Z. Z. Zhai, and Q. Zhou, *Curving the space by non-Hermiticity*, Nat. Commun. **13**, 2184 (2022).
- [83] J. S. Sun, C. A. Li, S. P. Feng, and H. M. Guo, *Hybrid higher-order skin-topological effect in hyperbolic lattices*, Phys. Rev. B **108**, 075122 (2023).
- [84] R. Shen, W. Chan, and C. H. Lee, *Non-Hermitian Skin Effect Along Hyperbolic Geodesics*, arXiv:2410.15278.
- [85] Note that saying a state Abelian or non-Abelian throughout this manuscript is in the sense of translational operations bringing a Bloch phase or not.

- [86] See Supplemental Material at [link](#) for further information on the geometry of hyperbolic lattices, details of the single-band model, and non-Hermitian non-Abelian semimetals.
- [87] P. Turbek, Algebraic curves, *Riemann surfaces and Klein surfaces with no non-trivial automorphisms or symmetries*. P. Edinburgh Math. Soc. **45**, 141 (2002).
- [88] F. Sausset and G. Tarjus, *Periodic boundary conditions on the pseudosphere*, J. Phys. A **40**, 12873 (2007).
- [89] Kittel, C. *Introduction to solid state physics*. 7th ed, (Wiley, 1996).
- [90] S. Weigert, *Completeness and orthonormality in symmetric quantum systems*, Phys. Rev. A **68**, 062111 (2003).
- [91] D. C. Brody, *Biorthogonal quantum mechanics*. J. Phys. A-Math. Theor. **47**, 035305 (2014).
- [92] I. Csiszar, *Geometry of Probability Distributions and Minimization Problems*, Ann. Probab. **3**, 146 (1975).
- [93] A. McDonald and A. A. Clerk, *Exponentially-enhanced quantum sensing with non-Hermitian lattice dynamics*, Nat. Commun. **11**, 5382 (2020).
- [94] W. T. Xue, M. R. Li, Y. M. Hu, F. Song, and Z. Wang, *Simple formulas of directional amplification from non-Bloch band theory*, Phys. Rev. B **103**, L241408 (2021).
- [95] Y. M. Hu and Z. Wang, *Green's functions of multiband non-Hermitian systems*, Phys. Rev. Res. **5**, 043073 (2023).
- [96] L. Xiao, W. T. Xue, F. Song, Y. M. Hu, W. Yi, Z. Wang, and P. Xue, *Observation of Non-Hermitian Edge Burst in Quantum Dynamics*, Phys. Rev. Lett. **133**, 070801 (2024).
- [97] G. Shankar and J. Maciejko, *Hyperbolic Lattices and Two-Dimensional Yang-Mills Theory*, Phys. Rev. Lett. **131**, 226401 (2024).
- [98] S. Hamanaka, A. A. Iliasov, T. Neupert, T. Bzdusek, and T. Yoshida, *Multifractal statistics of non-hermitian skin effect on the cayley tree*, arXiv:2408.11024.
- [99] J. Sun, C.-A. Li, S. Feng, and H. Guo, *Inner non-Hermitian skin effect on Bethe lattice*, arXiv:2409.07117.
- [100] J. Sun, C.-A. Li, Q. Guo, W. Zhang, S. Feng, X. Zhang, H. Guo, and B. Trauzettel, *Non-hermitian quantum fractals*, arXiv:2408.07355.
- [101] K. Y. Dixon, T. A. Loring, and A. Cerjan, *Classifying Topology in Photonic Heterostructures with Gapless Environments*, Phys. Rev. Lett. **131**, 213801 (2023).

[102] N. Chadha, A. G. Moghaddam, J. V. Brink, and C. Fulga, *Real-space topological localizer index to fully characterize the dislocation skin effect*, Phys. Rev. B **109**, 035425 (2024).

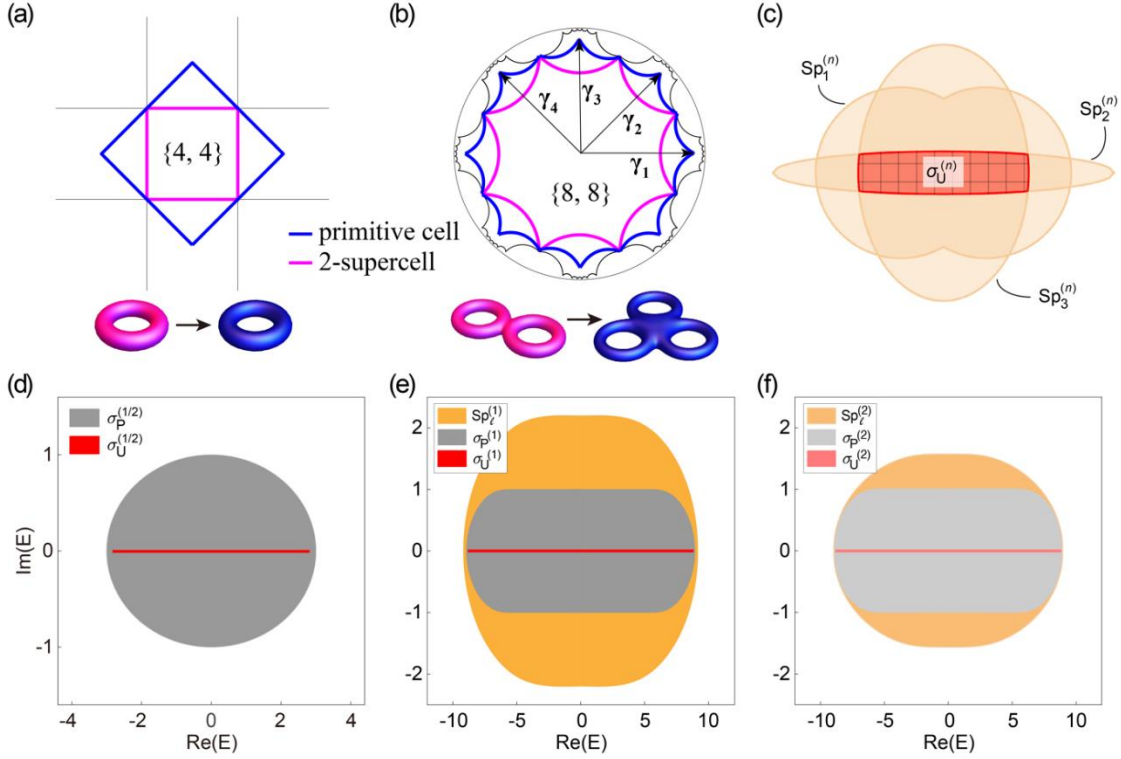


FIG. 1. (a,b) Symmetrized construction of n -supercells in (a) the Euclidean $\{4,4\}$ and (b) hyperbolic $\{8,8\}$ lattice. Translational operators $\{\gamma_i\}$ for each lattice are labeled herein. The corresponding translation groups are $\Gamma_{\{4,4\}}^{(1)} = \langle \gamma_1, \gamma_2 \mid \gamma_1 \gamma_2^{-1} \gamma_1^{-1} \gamma_2 = 1 \rangle$ and $\Gamma_{\{8,8\}}^{(1)} = \langle \gamma_1, \gamma_2, \gamma_3, \gamma_4 \mid \gamma_1 \gamma_2^{-1} \gamma_3 \gamma_4^{-1} \gamma_1^{-1} \gamma_2 \gamma_3^{-1} \gamma_4 = 1 \rangle$. The region enclosed by the magenta (blue) line at the top is the primitive cell (2-supercell), with its corresponding compactification sketched at the bottom. (c) Schematic illustration of our approach to calculate $\sigma_U^{(n)}$. $\text{Sp}_1^{(n)}$, $\text{Sp}_2^{(n)}$, and $\text{Sp}_3^{(n)}$ are depicted to represent all $\text{Sp}_\ell^{(n)}$, with their intersection (red hatched area) corresponding to $\sigma_U^{(n)}$. (d-f) $\sigma_P^{(n)}$ (grey areas) and $\sigma_U^{(n)}$ (red areas) for different supercells in (c) the $\{4,4\}$ and (d) $\{8,8\}$ lattice. The dark and light colors stand for the $n = 1$ and $n = 2$ cases, respectively. The orange areas in (e) and (f) display typical patterns of $\text{Sp}_\ell^{(n)}$ for $|\beta_j| = \{0.7, 0.7, 0.7, 0.7\}$ and $|\beta_j| = \{1.1, 1.2, 0.9, 1.2, 1.1, 0.8\}$, respectively. The EL model used is $H(\beta_1, \beta_2) = \beta_1 + \frac{1}{2}\beta_1^{-1} + \beta_2 + \frac{1}{2}\beta_2^{-1}$, while the HBL model is $H(\beta_1, \beta_2, \beta_3, \beta_4) = 2\beta_1 + \beta_1^{-1} + \beta_2 + \beta_2^{-1} + \beta_3 + \beta_3^{-1} + \beta_4 + \beta_4^{-1}$.

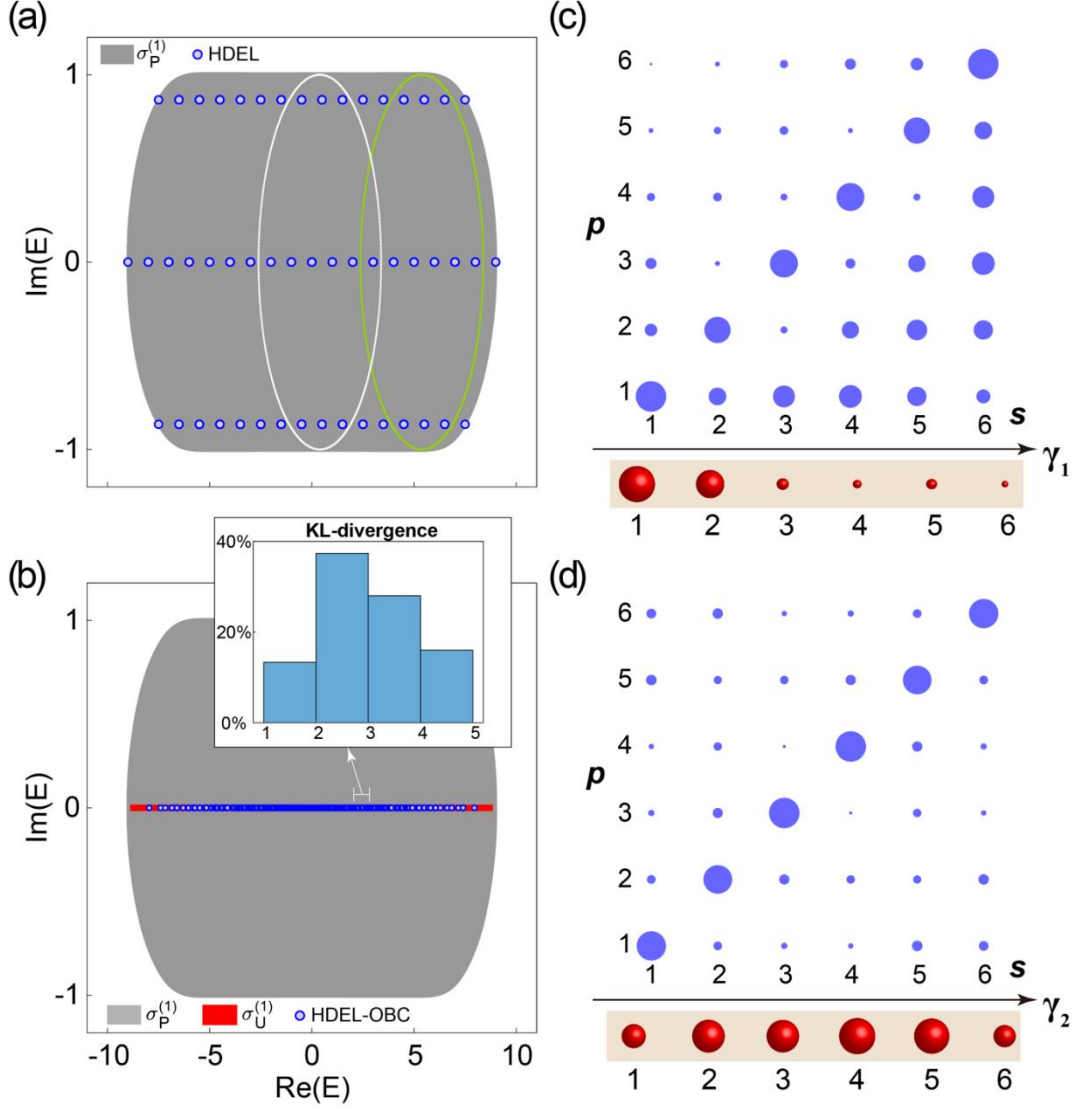


FIG. 2. (a,b) Spectra (blue circles) of (a) an HDEL and (b) the corresponding OBC configuration. The regions $\sigma_P^{(1)}$ and $\sigma_U^{(1)}$ are plotted in grey and red, respectively. The values of $\{k_2, k_3, k_4\}$ used in the white and green lines of (a) are $\{\pi/7, \pi/7, \pi/7\}$ and $\{\pi/4, 2\pi/3, \pi/2\}$, respectively. (c,d) Distribution of Green's functions (top panels) and the spectral sum of eigenstates (bottom panels) along (c) the γ_1 and (d) the γ_2 directions, with the marker sizes proportional to their magnitudes. The excitation energy is $E = 2.5$. The HDEL contains 1296 sites with explicit geometry defined in Sec. II of Ref. [86], and other parameters are the same as in Fig. 1.

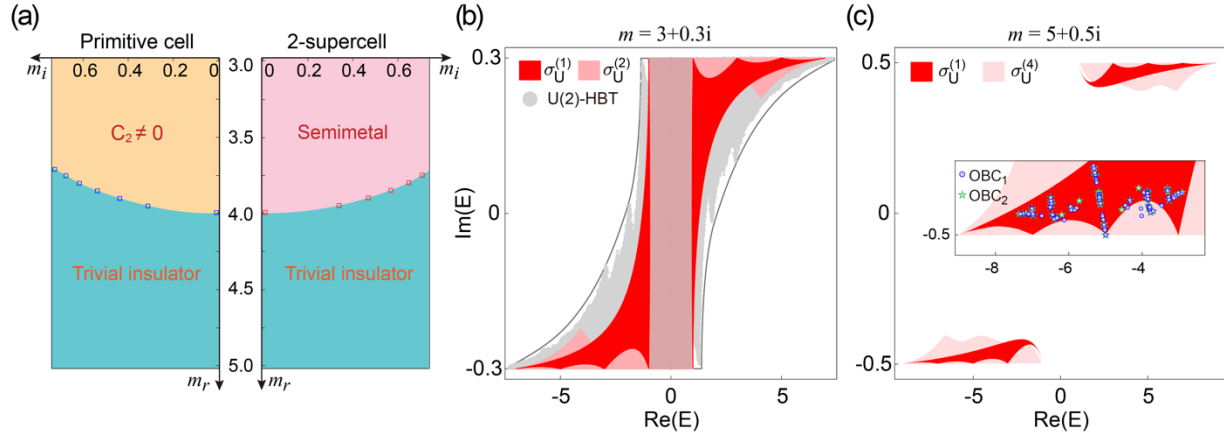


FIG. 3. (a) Phase diagram of the primitive cell (left) and 2-supercell (right) in the complex m plane. The regions in light orange and pink highlight the $C_2 \neq 0$ phase and semimetal phase, while the light cyan regions denote the trivial insulator phase. Blue and red squares represent the calculated phase transition points for the primitive cell and 2-supercell, respectively. (b) $\sigma_U^{(1)}$ (red) and $\sigma_U^{(2)}$ (light red) when $m = 3 + 0.3i$. The filled circles represent the spectra from U(2)-HBT by gathering 30 ensembles, and the dark solid line highlights their spectral boundary. (c) $\sigma_U^{(1)}$ (red) and $\sigma_U^{(4)}$ (light red) when $m = 5 + 0.5i$. The inset shows the lower branch of the spectra with the blue and green markers depicting the OBC spectra for two configurations consisting of 1601 and 1142 sites.